

1 Study of the Pulsar Wind Nebula HESS J1857+026 2 with Fermi-LAT

3 R. Rousseau, M.-H. Grondin, A. Van-Etten, M. Lemoine-Goumard, C. Espinoza, A.
4 Lyne, D. Smith, B. Stappers, and (J.-M. Casandjian)

5 (*Affiliations can be found after the references*)

6 Received /Accepted

7 ABSTRACT

8 *Context.* Since its launch in June 2008, the Fermi satellite has firmly identified 5 pulsar wind nebulae plus
9 a large number of candidates, all powered by young and energetic pulsars. HESS J1857+026 is an extended
10 gamma-ray source detected by H.E.S.S. during the Galactic Plane Survey and identified as the pulsar wind
11 nebula powered by the pulsar PSR J1856+0245.

12 *Aims.* We search for gamma pulsations from the pulsar PSR J1856+0245 and explore the characteristics of its
13 associated pulsar wind nebula.

14 *Methods.* Using a rotational ephemeris obtained with 76 observations made with the Jodrell Bank Telescope
15 at 1.520 GHz, we phase-fold 31 months of gamma-ray data acquired by the Large Area Telescope aboard
16 Fermi. We also perform a complete γ -ray spectral and morphological analysis.

17 *Results.* No pulsation is detected from PSR J1856+0245. However, significant emission is detected above
18 5 GeV at a position coincident with the TeV source HESS J1857+026. The gamma-ray spectrum is well
19 described by a simple power law with a spectral index of $\Gamma = 1.52 \pm 0.16 \pm 0.55$ and an energy flux of $G(100$
20 $\text{MeV} - 100 \text{ GeV}) = (2.72 \pm 0.58 \pm 1.51) \times 10^{-11} \text{ ergs/cm}^2/\text{s}$. This yields a γ -ray efficiency of $\sim 5\%$, in the
21 range expected for pulsar wind nebulae. Detailed multi-wavelength modeling bring new constraints on the
22 energetics and magnetic field of the pulsar wind nebula system.

Key words. Pulsar Wind Nebula - Plerion - Fermi-LAT - Gamma-Ray - HESS J1857+026 - PSR J1856+0245

23 1. Introduction

24 The dissipation of the rotational energy of a pulsar leads to the creation of a relativistic wind
25 made of electron/positron pairs. This inflating magnetized wind drives a shock and expands until
26 its pressure is balanced by that of the surrounding medium, which is often a Supernova Remnant
27 (SNR) (Gaensler et al. 2006). This phenomenon creates a Pulsar Wind Nebula (PWN).

28 Since 2003, the continuous observations of the Galactic Plane by Čerenkov telescopes (espe-
29 cially HESS¹ but also VERITAS and MAGIC) have yielded the detection of more than 60 Galactic
30 sources. Among them, PWN is the dominant class with 28 sources firmly identified. In the GeV
31 energy range, 5 PWNe have been firmly identified using Fermi-LAT data. All are powered by
32 energetic pulsars and their γ -efficiencies are $\sim 1\%$ consistent with TeV observations by HESS

¹ <http://www.mpi-hd.mpg.de/hfm/HESS/pages/home/sources/>

33 (Ackermann et al. 2011; Grondin et al. 2011a). Furthermore Fermi-LAT has detected an increas-
 34 ing population of pulsars (96) as well as new PWNe candidates and provides new constraints on
 35 radiation processes (Abdo et al. 2010a; Pellizzoni et al. 2010).

36 The presence of a pulsar close to the source position is an important clue to confirm the identifi-
 37 cation of a PWN, which often requires information from the radio/X-ray wavelengths. The radio/X-
 38 ray PWNe are often associated with TeV extended sources slightly offset from their pulsars. This
 39 offset can be explained by taking into account the inhomogeneous environment leading, for in-
 40 stance, to an asymmetric PWN (Hinton et al. 2010). In such sources, TeV radiation can be ex-
 41 plained by Inverse Compton (IC) scattering of an old population of leptons produced earlier in
 42 the pulsar’s life on ambient photon fields (CMB, IR, ...) or by π^0 decay from the interaction of
 43 accelerated hadrons with nuclei of the interstellar medium.

44 HESS J1857+026 is a very high energy (VHE) gamma-ray source detected by HESS during
 45 the Galactic Plane Survey (Aharonian et al. 2008) and later detected by MAGIC (Klepser et al.
 46 2011). The extended ($\sim 0.11^\circ$) TeV source was identified as a PWN after the discovery of PSR
 47 J1856+0245 (offset $\sim 0.12^\circ$) in the Arecibo PALFA survey (Hessels et al. 2008). PSR J1856+0245
 48 is an energetic pulsar ($\dot{E} = 4.6 \times 10^{36} \text{ erg/s}$) located in a dense region, 1.3° from the bright SNR
 49 W44 (Abdo et al., 2010) and 0.6° from the fainter SNR HESS J1858+020 on which only an
 50 upperlimit could be set using Fermi data (Torres et al. 2011). Interestingly, significant emission
 51 coincident with HESS J1857+026 was observed above 100 GeV using Fermi-LAT data (Neronov
 52 et al. 2010).

53 Here, we report in details GeV observations of the HESS J1857+026/PSR J1856+0245 system
 54 with Fermi-LAT.

55 2. LAT description and data selection

56 The LAT is a gamma-ray telescope that detects photons by conversion into electron-positron pairs
 57 and operates in the energy range between 20 MeV and 300 GeV. Details of the instrument and data
 58 processing are given in Atwood et al., (2009). The on-orbit calibration is described in Abdo et al.
 59 (2009a).

60 The following analysis was performed using 36 months of data collected starting August 4,
 61 2008, and extending until August, 31, 2011. Only gamma-rays in the Pass 7 Source class events
 62 were selected from this sample, we excluded those coming from a zenith angle larger than 100°
 63 because of the possible contamination from secondary gamma-rays from the Earth’s atmosphere
 64 (Abdo et al. 2009b). We have used the P7 V6 Instrument Response Functions (IRFs). We selected
 65 the ‘Source’ events which correspond to a compromise between the number of selected photons
 66 and the background rate, following the procedure described on the Fermi Science Support Center².

67 3. Data analysis

68 3.1. Timing analysis of PSR J1856+0245

69 With its large spin-down power, the pulsar PSR J1856+0245 is one of the more energetic known
 70 radio pulsars. Its spin period of 80.9 ms and characteristic age of 20.6 kyr are similar to those of

² FSSC: <http://fermi.gsfc.nasa.gov/ssc/data/access/lat/ephems/>

71 the Vela pulsar. The dispersion measure and NE2001 electron density model of the Galaxy assign
72 PSR J1856+0245 a distance of ~ 9 kpc (Cordes et al. 2002).

73 This pulsar is not monitored as part of the LAT pulsar timing campaign (Smith et al. 2008) but
74 has been regularly observed with the Jodrell Bank Telescope (Hobbs et al. 2004).

75 The ephemeris of the pulsar PSR J1856+0245 used in the analysis of the *Fermi*-LAT data was
76 obtained using 76 observations at 1.520 GHz made with the Jodrell Bank Telescope between 2008
77 May 4 and 2011 April 15. The arrival times of events were corrected to the Solar System Barycenter
78 using the JPL DE405 Solar System ephemeris.

79 The TEMPO2 timing package (Hobbs et al. 2008) was then used to build the timing solution.
80 We fit the radio times of arrival (TOAs) to the pulsar rotation frequency and first four derivatives.
81 The post-fit rms is 1.182 ms, or 1.5 % of the pulsar phase. This timing solution will be made
82 available through the FSSC.

83 Photons with energies above 100 MeV and within a radius of 1.0° of the pulsar radio po-
84 sition ($\alpha(\text{J2000}) = 18^{\text{h}}56^{\text{m}}50.937^{\text{s}}$, $\delta(\text{J2000}) = +02^\circ45'47.046''$), were selected using a energy-
85 dependent cone of radius $\theta_{68} < \max(5.12^\circ \times (E/100 \text{ MeV})^{-0.8}, 0.2^\circ)$ and phase-folded using the
86 radio ephemeris previously described. This choice takes into account the instrument performance
87 and maximizes the signal to noise ratio over a broad energy range.

88 The H-Test values, as defined in De Jager et al. (2009) and obtained from the pulsed analysis,
89 correspond to a significance well below 2σ for each tested energy band (100 MeV – 300 GeV, 100
90 MeV – 300 MeV, 300 MeV – 1 GeV, > 1 GeV). No significant pulsation is detected.

91 3.2. Spatial and spectral analysis

92 Two different tools were used to perform the spatial and spectral analysis : `gtlike` and `pointlike`.
93 `gtlike` is the maximum-likelihood method (Mattox et al. 1996) implemented in the science tools
94 distributed by the FSSC. This tool fits a source model to the data along with models for the in-
95 strumental, extragalactic and Galactic components of the background. In the following analysis,
96 the Galactic diffuse emission is modeled by the ring–hybrid model `gal_2yearp7v6_v0.fits`. The in-
97 strumental background and extra-galactic radiation are described by a single isotropic component
98 with a spectral shape described by the tabulated model `iso_p7v6source.txt`. The models and their
99 description have been released by the Fermi Collaboration through the FSSC website.

100 `pointlike` is a binned likelihood technique that was extensively tested against `gtlike`. It
101 convolves the intrinsic LAT PSF with a spatial model of the candidate source to create a “Pseudo-
102 PSF” of the source appearance (Kerr 2011). `pointlike` can be used to assess the Test Statistic
103 (TS) value and derive the shape and spectra of both point-like and extended sources.

104 The TS estimates the significance and is defined as $TS = 2(L_1 - L_0)$ were L_1 corresponds to
105 the log-likelihood obtained by fitting a source model of the source of interest plus the background
106 model to the data and L_0 correspond to the log-likelihood obtained by fitting the background model
107 only (Wilks 1938).

108 Sources in a region of 10° around HESS J1857+026 were extracted from the Second Fermi-
109 LAT catalog (Abdo et al. 2011) and taken into account in this study, fixing their spectral parameters
110 if they are more than 5° from our source of interest.

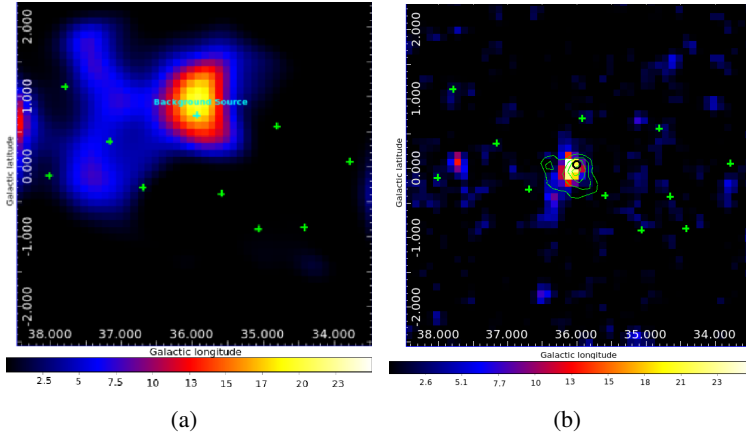


Fig. 1. Residual TS map obtained by fitting a source at each location of the map and computing the TS using `pointlike`. The green crosses represents the sources of the 2FGL catalog all included in the model. **(a):** Residual TS map obtained between 100 MeV and 1.3 GeV. This figure shows a residual excess taken into account in our model by adding a source to the model. **(b):** Residual TS map obtained between 10 GeV and 300 GeV. Here HESS J1857 is not included in the model. The green contours are those obtained using HESS data (Aharonian et al., 2008). The position of the Fermi excess is consistent with those of HESS. The black circle represents the position of PSR J1856+0245.

111 The region analyzed here includes the bright SNR W44, known to interact with its environ-
112 ment. Extended and only 1.3° from HESS J1857+026, W44 could influence our fit. We refitted it
113 assuming an elliptical ring and obtained results consistent with those of Abdo et al. (2010b).

114 3.2.1. Shape and position of the source

115 Source shape analysis requires the best possible angular resolution. Since the source has a hard
116 spectrum (see Section 3.2.2) we made a compromise between statistics and resolution by select-
117 ing photons above 10 GeV. This also drastically reduces the contribution of the Galactic diffuse
118 background. Fig. 1(b) presents a LAT TS Map in the energy range 10 GeV-100 GeV. The skymap
119 contains the TS value for a point source at each map location, thus giving a measure of the statisti-
120 cal significance for the detection of a γ -ray source in excess of the background. A source coincident
121 with HESS J1857+026 is clearly visible.

122 We determined the shape of the source using `pointlike` with three different models : a point
123 source, a uniform disk and a Gaussian. No significant extension was obtained above 10 GeV. The
124 best model for HESS J1857+026 is a point source located at the position $\alpha(J2000) = 18^h57^m14.4^s$
125 , $\delta(J2000) = +02^\circ45'36.0''$ consistent with the position determined by HESS ($\alpha(J2000) =$
126 $18^h56^m50.80^s$, $\delta(J2000) = +02^\circ45'50.2''$).

127 3.2.2. Spectral analysis

128 Fig. 1(a) shows a TS map of the region in the energy range 0.1-1.3 GeV. An emission excess appears
129 close to HESS J1857+026. Located at ($\alpha(J2000) = 18^h54^m19.2^s$, $\delta(J2000) = +02^\circ59'13.0''$), this
130 excess cannot be explained by HESS J1857+026 and was added to the model of the region.

131 The spectral analysis was done using `gtlike` selecting photons only between 300 MeV and
132 300 GeV since the low energy range is dominated by the diffuse Galactic background and subject

133 to systematics. In this energy range, HESS J1857+026 is well described by a pure power-law with
 134 an integrated flux extrapolated down to 100 MeV of $F(100 \text{ MeV}-100 \text{ GeV})=(5.79 \pm 0.75 \pm 3.11) \times$
 135 $10^{-9} \text{ ph/cm}^2/\text{s}$, a spectral index of $\Gamma = 1.52 \pm 0.16 \pm 0.55$ and an energy flux of $G(100 \text{ MeV}-100$
 136 $\text{ GeV})=(2.72 \pm 0.58 \pm 1.51) \times 10^{-11} \text{ ergs/cm}^2/\text{s}$ leading to a significance of $\sim 6\sigma$ (TS=38.7).

137 The additional background source was fitted assuming a logarithmic parabola (eq. 2 in Abdo
 138 et al. (2011)), with spectral parameters $\alpha = 3.5 \pm 0.2_{stat}$, $\beta = 0.6 \pm 0.1_{stat}$, $E_0 \sim 1.2 \text{ GeV}$, and
 139 $K = (3.1 \pm 0.5_{stat}) \times 10^{-12} \text{ ph/MeV/cm}^2/\text{s}$. Its significance above 300MeV is $\sim 4.6\sigma$.

140 Fermi-LAT spectral points for HESS J1857+026 were obtained by dividing the 300 MeV-300
 141 GeV range into 4 logarithmically-spaced energy bins, as presented in Fig. 2. Both statistical and
 142 systematic errors were estimated and added in quadrature yielding the red error bars.

143 Three main systematic uncertainties can affect the LAT flux estimate for a point source: uncer-
 144 tainties in the Galactic diffuse background, uncertainties on the effective area and uncertainties on
 145 the shape of the source. The dominant uncertainty at low energy comes from the Galactic diffuse
 146 emission, estimated by changing the normalization of the Galactic diffuse model artificially by 6%
 147 as done in (Abdo et al., 2010). The second systematic is estimated by using modified IRFs whose
 148 effective areas bracket those of our nominal IRF as in (Grondin et al. 2011b). The fact that we do
 149 not know the true gamma-ray morphology introduces a last source of error. We derived an estimate
 150 of the uncertainty on the shape of the source by using the best Gaussian model obtained by HESS.
 151 We combine this various errors in quadrature to obtain our best estimate of the total systematic
 152 error at each energy and propagate through to the fit model parameters.

153 As for other PWNe detected by Fermi, HESS J1857+026 is powered by a young (Age < 21
 154 kyrs) and energetic pulsar. Assuming a distance of 9kpc, the γ -ray flux obtained using Fermi-LAT
 155 data of $L_{PWN}^{\gamma} = 2.49 \times 10^{35} \text{ ergs/s}$. This yields to a γ -ray efficiency of $\sim 5 \%$. According to Fig. 7
 156 of Ackermann et al. (2011), this is one of the highest PWN efficiencies observed in the GeV range
 157 by Fermi. It is still in the range of expected values and confirms the trend observed in the TeV band
 158 (3.1 %) using the HESS data (Mattana et al. 2009; Marandon et al. 2010).

159 Using our best model describing the region, we derived an upper limit on the DC emission of
 160 the pulsar. Following the procedure used by Romani et al. (2011), we added a point source at the
 161 position of the pulsar assuming a power-law of index 1.62 and a cut-off energy at 2.8 GeV. No
 162 significant signal was obtained leading to a 99% upper limit on the flux of $6.22 \times 10^{-12} \text{ erg/cm}^2/\text{s}$.
 163 Assuming a distance of 9 kpc for the pulsar, this implies a limit on the γ -ray luminosity of $7.47 \times$
 164 10^{34} erg/s .

165 4. Discussion

166 To investigate the global properties of the PWN, we apply a one-zone time dependent SED model,
 167 as described in Grondin et al. (2011b) and Abdo et al. (2010a). This model computes SEDs from
 168 evolving electron populations over the lifetime of the pulsar in a series of time steps, with the energy
 169 content of the injected particle population varying with time following the pulsar spin down. During
 170 the free-expansion phase of the PWN (assumed to be $\sim 10^4$ years) we adopt an expansion of $R \propto t$,
 171 following which the radius $R \propto t^{0.3}$, appropriate for a PWN expanding in pressure equilibrium with
 172 a Sedov phase SNR. Over the pulsar lifetime the magnetic field $B \propto t^{-1.5}$, following ~ 500 years of
 173 constancy. At each time step synchrotron, inverse-Compton (Klein-Nishina effects included), and

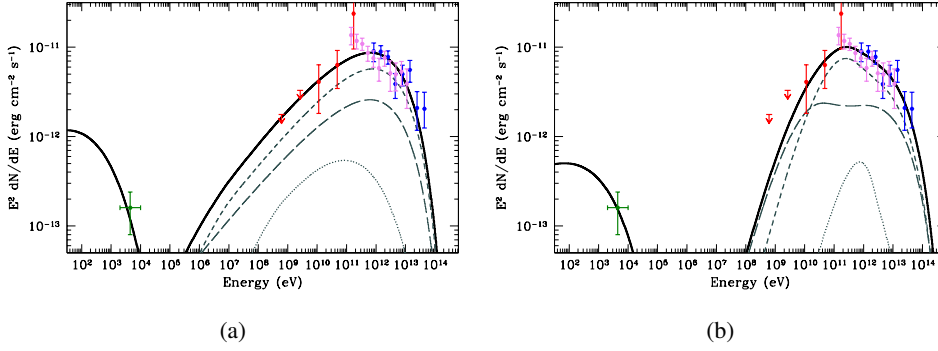


Fig. 2. Spectral energy distribution of HESS J1857+026 with a simple exponentially cutoff power-law electron spectrum (a), and a relativistic Maxwellian plus power-law electron spectrum (b). The X-ray flux point (green), LAT spectral points (red), MAGIC points (violet) (Klepser et al. 2011), and H.E.S.S. points (blue) (Aharonian et al. 2008) are shown. The black line denotes the total synchrotron and inverse Compton emission from the nebula. Thin curves indicate the Compton components from scattering on the CMB (long-dashed), IR (medium-dashed), and stellar (dotted) photons.

174 adiabatic losses are calculated. Synchrotron and IC fluxes are calculated from the final electron
175 spectrum. We fix the pulsar braking index to the canonical value of 3, and allow the initial spin
176 period P_0 of the pulsar to vary, thereby changing the age and spin-down behavior of the pulsar.

177 We assume the existence of three primary photon fields (CMBR, far IR (dust), and starlight) and
178 use the interstellar radiation mapcube within the GALPROP suite (Porter et al. 2005) to estimate
179 the photon fields at the Galactic radius of PSR J1856+0245. A distance of 9 kpc in the direction of
180 the pulsar corresponds to a Galactic radius of 5.4 kpc. At this radius, the peak of the SED of dust
181 IR photons corresponds to a black body temperature of $T \sim 32$ K with a density of ~ 1.1 eV cm $^{-3}$,
182 while the SED of stellar photons peaks at $T \sim 2500$ K with a density of ~ 1.2 eV cm $^{-3}$.

183 Spectral measurements consist of LAT, MAGIC (Klepser et al. 2011) and H.E.S.S. (Aharonian
184 et al. 2008) data points, as well as an estimate of the X-ray flux. Hessels et al. (2008) estimate a
185 2–10 keV flux of 1.6×10^{-13} erg cm $^{-2}$ s $^{-1}$ for the faint ASCA source AX J185651+0245 coincident
186 with the pulsar. We assign 50% error bars to this very rough estimate. Hessels et al. (2008) also
187 estimate a non-constraining 1.4 GHz radio upper limit of $\sim 1.8 \times 10^5$ Jy sr $^{-1}$.

188 A simple exponentially cutoff power-law injection of electrons, evolved properly over the pulsar
189 lifetime, often provides an adequate match to PWNe SEDS. Initially, we fit this injection spectrum
190 with five variables: final magnetic field $B_f = 2.1 \pm 1.0$ μ G, electron high energy cutoff $E_{\text{cut}} = 59 \pm 17$
191 TeV, electron power-law index $p = 2.15 \pm 0.03$, initial pulsar spin period $P_0 = 10 \pm 6$ ms, and
192 pulsar braking index $n = 3.0$, which gives an age of 20 kyr. This simple injection spectrum yields
193 a $\chi^2/dof = 24.8/21$ and cannot match the low energy MAGIC points or highest energy H.E.S.S.
194 points, as shown in Figure 2 (Top).

195 Another option to fit the multi-wavelength data is to adopt the relativistic Maxwellian plus
196 power-law tail electron spectrum proposed by Spitkovsky (2008). We implement this spectrum as
197 described in Grondin et al. (2011b). The best fit, presented in Figure 2 (Bottom), is obtained with
198 $kT = 0.72 \pm 0.09$ TeV, corresponding to an upstream gamma-factor of 2.8×10^6 , a magnetic field
199 of $B_f = 1.5 \pm 0.8$ μ G, a cutoff at $E_{\text{cut}} = 140 \pm 71$ TeV and a power-law index of $p = 2.49 \pm 0.10$,
200 consistent with the value of ~ 2.5 proposed by Spitkovsky (2008). The braking index of $n = 3$ and

201 initial spin period of $P_0 = 42 \pm 5$ ms give an age of 15 kyr. The relativistic Maxwellian plus power
 202 law model better matches the multi-wavelength data, with a $\chi^2/dof = 13.6/21$ and also directly
 203 probes the upstream pulsar wind via fitting of γ_0 . The low magnetic field of the fit is due almost
 204 entirely to the low X-ray flux measurement, and deeper X-ray observations will hopefully improve
 205 this estimate. The MAGIC and H.E.S.S. data combine to form a power-law spectra of index ~ 2.3
 206 over nearly 3 decades in energy. This VHE data (combined with the limits imposed by the LAT
 207 data) is difficult to match with a simple power-law injection of electrons, and we find a significantly
 208 better fit with a relativistic Maxwellian plus power-law spectrum. Previous SED modeling papers
 209 have shown that in some cases the addition of a relativistic Maxwellian component improves the
 210 match between model and data (Fang et al. 2010; Slane et al. 2010; Grondin et al. 2011b).

211 Acknowledgements

212 The Fermi-LAT Collaboration acknowledges generous ongoing support from a number of agencies
 213 and institutes that have supported both the development and the operation of the LAT as well as
 214 scientific data analysis. These include the National Aeronautics and Space Administration and the
 215 Department of Energy in the United States, the Commissariat à l'Energie Atomique and the Centre
 216 National de la Recherche Scientifique / Institut National de Physique Nucléaire et de Physique des
 217 Particules in France, the Agenzia Spaziale Italiana and the Istituto Nazionale di Fisica Nucleare in
 218 Italy, the Ministry of Education, Culture, Sports, Science and Technology (MEXT), High Energy
 219 Accelerator Research Organization (KEK) and Japan Aerospace Exploration Agency (JAXA) in
 220 Japan, and the K. A. Wallenberg Foundation, the Swedish Research Council and the Swedish
 221 National Space Board in Sweden.

222 The Lovell Telescope is owned and operated by the University of Manchester as part of the
 223 Jodrell Bank Centre for Astrophysics with support from the Science and Technology Facilities
 224 Council of the United Kingdom.

225 References

- 226 A. Abdo et al., *ApJ*, 696, 2, 1084-1093, 2009 a
 227 A. Abdo et al., *Phys. Rev. D*, 80, 122004, 2009 b
 228 A. Abdo et al., *ApJ*, 713, 146, 2010 a
 229 A. Abdo et al., *Science*, 327, 1103-1106, 2010 b
 230 A. Abdo et al., *ApJS*, Submitted, 2011
 231 M. Ackermann et al., *ApJ*, 726, 35, 2011
 232 F. Aharonian et al., *A&A*, 477, 353, 2008
 233 W. Atwood et al., *ApJ*, 697, 2, 1071-1102, 2009
 234 J. Cordes, T. Lazzio, arXiv:astro-ph/0207156
 235 J. Fang, & Zhang, L. *A&A*, 515, A20, 2010
 236 O. De Jager et al., *A&A*, 221, 180, 1989
 237 B. Gaensler, P. Slane, *Ann. Rev. of A & A*, 44, 17-47, 2006.
 238 M.-H. Grondin, M. Lemoine-Goumard, *Heep conf.*, A.S.S.P., 399-411, 2011 a
 239 M.-H. Grondin et al., *ApJ*, 738, 42, 2011 b
 240 J.A. Hinton and W. Hofmann, *Ann. Rev. A& A*, 47, 523-565, 2010
 241 G. Hobbs et al., *MNRAS* 353, 1311, 2004
 242 G. Hobbs et al., *Chin. J. A A*, 6, 2, 189, 2006
 243 J. Hessels et al., *ApJ*, 682, L41L44, 2008

244 M. Kerr, arXiv:1101.6072v
245 S. Klepser et al., proc. 32 ICRC
246 V. Marandon et al., thesis, 2010
247 F. Mattana et al., ApJ, 694, 12-17, 2009
248 J. Mattox et al., ApJ, 461, 396-407, 1996
249 A. Neronov et al., arXiv:1011.0210v1
250 A. Pellizzoni et al., Science, 327, 663, 2010
251 T. A. Porter et al., International Cosmic Ray Conference, 4, 77, 2005
252 R. Romani et al., arXiv:1106.5762v1
253 P. Slane et al., ApJ, 720, 266, 2010
254 D. Smith et al., A&A, 492, 3, 923-931, 2008
255 A. Spitkovsky, ApJ, 682, L5, 2008
256 D. Torres et al., arXiv:1107.3470
257 S. Wilks, Ann. Math. Stat., 9, 60, 1938

258 ¹ Corresponding authors : R. Rousseau (rousseau@cenbg.in2p3.fr), M. Lemoine-Goumard
259 (lemoine@cenbg.in2p3.fr), A. Van Etten (ave@stanford.edu)
260 ² Université Bordeaux 1, CNRS/IN2P3, Centre d'Études Nucléaires de Bordeaux Gradignan, 33175
261 Gradignan, France
262 ³ Funded by contract ERC-StG-259391 from the European Community
263 ⁴ Max-Planck-Institut für Kernphysik, Saupfercheckweg 1, 69117 Heidelberg, Germany
264 ⁵ Landessternwarte, Universität Heidelberg, Königstuhl, 69117 Heidelberg, Germany
265 ⁶ W. W. Hansen Experimental Physics Laboratory, Kavli Institute for Particle Astrophysics and Cosmology,
266 Department of Physics and SLAC National Accelerator Laboratory, Stanford University, Stanford, CA
267 94305, USA